CHARLES UNIVERSITY IN PRAGUE

Faculty of Science

Department of Physical and Macromolecular Chemistry

Program: Physical chemistry

Jana Hajduová

ASOCIACE POLY(4-HYDROXYSTYREN)-*b*-POLY(ETHYLENOXID)U A JEHO DERIVÁTŮ

SELF-ASSEMBLY OF POLY(4-HYDROXYSTYRENE)-BLOCK-POLY(ETHYLENE OXIDE) COPOLYMER AND ITS DERIVATIVES

Diploma Thesis

Supervisor: RNDr. Miroslav Štěpánek, Ph.D.

Prague 2012

Title: Self-assembly of poly(4-hydroxystyrene)-block-poly(ethylene oxide) copolymer and its derivatives

Annotation: This thesis is based on studies of self-assembly of double hydrophilic block copolymers, consisting of poly(ethylene oxide) as the neutral water soluble block, and a second polyelectrolyte block consisting of derivatives of poly(4-hydroxystyrene). The study was aimed at characterization of behavior in different solvents, preparation of the nanoparticles and description of the interaction with ionic surfactants by an experimental study using the combination of several scattering and microscopic techniques.

Key words: double hydrophilic block copolymers, self-assembly, surfactant

Název: Asociace poly(4-hydroxystyren)-*b*-poly(ethylenoxid)u a jeho derivátů

Anotace: Táto práce je založena na studiu asociace dvoublokových hydrofilních kopolymerů skládajících se z poly(ethylenoxid)u, jakožto neutrálního ve vodě rozpustného bloku, a polyelektrolytového bloku skládajícího se z derivátů poly(4-hydroxystyren)u. Studium bylo zaměřeno na charakterizaci chování v různých rozpouštědlech, přípravu nanočástic a popis interakcí s iontovými surfaktanty prostřednictvím různých rozptylových a mikroskopických měření.

Klíčová slova: dvoublokové hydrofilní kopolymery, samoskladba, surfaktant

This thesis was elaborated in connection with the research plan MSM0021620857 “New molecular systems for the advanced health beneficial and environmentally friendly applications”.

I declare that I have elaborated the thesis on my own. If already published results are used, they are included in the list of references. I agree with lending the thesis to anyone who may be interested. It is not substantially the same as any work that has been or is being submitted to any other University for any degree, diploma or any other qualification.

Prague, 13.4.2012

I would like to thank to my supervisor RNDr. Miroslav Štěpánek, Ph.D. for vocational guidance, assistance, inspiring discussions, comments, suggestions and patience in creating this diploma thesis. I would also like to thank to RNDr. Miroslav Šlouf, Ph.D., Institute of Macromolecular Chemistry, Academy of Sciences of the Czech Republic and to Ing. Jana Nebesářová, CSc., Biology Centre − Institute of Parasitology, Academy of Sciences of the Czech Republic for TEM and Cryo-FESEM measurements.

Special thanks belong to my family and friends for their support.

Contents

Abbreviations

cmc	critical micelle concentration
cmt	critical micelle temperature
PPO	poly(propylene oxide)
Cryo-FESEM	cryogenic field-emission scanning electron microscopy
DTAB	dodecyl trimethylammonium bromide
NMR	nuclear magnetic resonance
NPHOS	poly [3,5-bis(dimethylaminomethyl)-4-hydroxystyrene]
PAA	poly(acrylic acid)
PBA	poly(n-butyl acrylate)
PDEGA	poly(diethylene glycol ethylether acrylate)
PEO	poly(ethylene oxide)
PHOS	poly(4-hydroxy styrene)
PPO	poly(propylene oxide)
PS	poly(styrene)
PSS	poly(styrene sulfonate)
PtBS	poly(tert-butylstyrene)
PtBOS	poly(tert-butoxystyrene)
QNPHOS	poly [3,5-bis(trimethylammoniummethyl)-4-hydroxystyrene iodide]
R_g	radius of gyration
R_H	hydrodynamic radius
SDS	sodium dodecyl sulfate
SLS	static light scattering
TEM	transmission electron microscopy
T_g	glass transition temperature
THF	tetrahydrofuran
β	stoichiometric ratio
γ	interfacial tension

1 MOTIVATION OF THE STUDY AND AIM OF THE THESIS

Polymer mixtures containing block copolymers that exhibit fascinating self-assembly behavior have attracted much attention for the use as functional nanostructures. Block copolymer micelles find a number of advanced applications, for example as drug carrier vessels in targeted delivery systems and controlled drug release. Despite a large amount of successful results and achieved knowledge in recent years, there are still needs for the study of new systems and optimization of ways of the preparation new polymeric nanoparticles.

This thesis is focused on the study of self-assembled nanostructures formed by double-hydrophilic block copolymers based on poly(4-hydroxystyrene) derivatives and poly(ethylene oxide), obtained in the framework of international collaboration of our laboratory. One of the goals of this work is to demonstrate the differences in behavior between copolymer containing block of poly(4-hydroxystyrene) itself and copolymers with its 3,5-bis(dimethylaminomethyl) and 3,5-bis(trimethyl-ammoniummethyl) derivatives, respectively.

The studies of the copolymers were aimed at detailed characterization of their association behavior in different solvents, preparation of the nanoparticles and description of the interaction with ionic surfactants using a combination of scattering and microscopic techniques.

2 INTRODUCTION

2.1 SELF-ASSEMBLY OF BLOCK COPOLYMERS IN SOLUTION

Supramolecular assemblies of block copolymers have received considerable attention from both fundamental and applied standpoints. One of the most intensively studied topics in the developing field of self-assembled block copolymers is the polymeric micelles formed in aqueous media from amphiphilic block copolymers. An amphiphilic block copolymer in a selective solvent, which is a good solvent for one of the blocks and a precipitant for the other, self-assembles by a closed association process into well-defined aggregates. The process of aggregation starts above the critical micelle concentration (CMC) and above or below critical micelle temperature (CMT). It has been found that structural and thermodynamic parameters such as CMC, the association number of the copolymers in the micelles, and the size of the micelles depend on the selectivity of the solvents, composition of the mixed solvents, the ionic strength, the temperature, the polymer concentration, the molecular weight of the copolymer, the length of the blocks, and the sequence of the blocks [1-3]. pH-dependent behavior of block copolymers has also been studied [4]. The assemblies may assume various morphologies, including spherical, rod and lamellar structures. Various kinds of amphiphilic block copolymers have so far been synthesized, and their self-assembly behavior has been investigated intensively from the physicochemical viewpoint. Most investigations deal with nanoparticles of AB diblock and ABA- or BAB-type triblock copolymers, where A is a hydrophobic, core-forming block, and B is a hydrophilic, shell-forming block.

Water is a strong precipitant for all hydrophobic polymers, so that the copolymers, which contain a long hydrophobic block, are not directly soluble in water. Nevertheless, the aqueous solutions of polymeric nanoparticles can be prepared indirectly by dissolution in common solvent of both blocks or in a mild selective

solvent for the block with higher polarity, usually in a mixture of a good (organic) solvent for the hydrophobic block and water. The organic cosolvent can be later removed by dialysis against water.

Typical block copolymers that self-assemble in an aqueous medium, are copolymers of poly(ethylene oxide) PEO and poly(propylene oxide) PPO. Their trade name is Pluronics and their association behavior has been studied since the 1970s [5, 6]. Various experimental techniques, including small neutron scattering, small angle X-ray scattering, fluorescence, scanning calorimetry, static and dynamic light scattering, stress relaxation and pulsed field gradient NMR have been utilized in study of aqueous PEO-PPO-PEO block copolymers. The association behavior of the PEO-PPO-PEO is governed by the interplay between the hydrophobicity and hydrophilicity of the building blocks and their interactions with polar solvent water. Both PEO and PPO blocks show hydrophilicity at low temperatures and enhanced hydrophobicity at higher temperatures. The temperature-induced hydrophobicity of PPO is stronger than for PEO, and therefore PPO tends to aggregate to avoid contact with water molecules.

In dilute and moderately concentrated solutions, a temperature increase indicates micellization, where the copolymer chains associate to form micelles consisting of a core of PPO with a water-swollen mantle of PEO chains. The general trend is that the critical micelle concentration (cmc) decreases with increasing temperature or with increasing weight fraction of the hydrophobic PPO block [7].

A series of investigations has been recently conducted by showing that self-assembly of surfactants and block copolymers occurs also in a variety of selective organic solvents [8-13]. Alexandridis and Yang have revealed that PEO-PPO-PEO block copolymers self-assemble in formamide [9]. Katime and coworkers have systematically studied block copolymers of polystyrene-poly(ethylene-propylene) (PS-PEP) and polystyrene-poly(ethylene-butylene) (PS-PEB) in a wide range of organic solvents [10-13]. It was found, that self-assembly behavior depends on polarity of the solvent. Some organic solvents, for example formamide, are polar enough to present similarities with aqueous solutions. Micellization in formamide, similar to what is observed in aqueous solution, is followed by an increase in enthalpy, being therefore, driven by the accompanying entropy increase [9]. On the other hand, a general behavior for micellization in apolar organic solvents

indicates that aggregation is driven by enthalpy changes, attributed to the balance between segment-solvent and segment-segment interactions. In a selective solvent, the poorly solvated block replaces its interaction with the solvent for one with the identical blocks, forming the segregated micelle core, whereas the selective solvent remains interacting with the other block forming the swollen corona. This results in a favorable overall energetic balance, hence an exothermic process. Concomitantly, there is an entropy decrease due to restraint of chain mobility upon aggregate formation, but not enough to overcome the favorable enthalpy decrease, leading to a negative Gibbs energy change and a thermodynamically favorable process.

2.2 POLYELECTROLYTE BLOCK COPOLYMERS

As for nonionic block copolymers, micellization of polyelectrolyte block copolymers occurs in a solvent that is selective for one of the block. However, the ionic character introduces new parameters governing the structure and properties of the micellar solution. The strength of the polyelectrolyte plays an important role in micellization in polyelectrolyte-containing copolymers. In strongly charged polyelectrolytes, such as poly(styrene sulfonate), the ionic units are essentially fully dissociated, irrespective of ionic strength or pH. Polyelectrolytes in which the number and arrangement of charges is fixed are termed “quenched” polyelectrolytes. In “annealed” polyelectrolytes the degree of dissociation depends on pH, as the total number and position of charges is not fixed.

The ionic strength plays an important role in the chain conformation of polyelectrolytes, and the presence of a high charge density leads to some specific properties unique to ionic block copolymers. Many of the studies on ionic block copolymers have been undertaken with solvents selective for the ionic polyelectrolyte block, generally aqueous solutions, despite it has been observed that it is often difficult to dissolve hydrophilic-hydrophobic block copolymers in water. Process of the dissolution of copolymer in mild solvent and subsequent dialysis against water can influence the charge and hence conformation of the polyelectrolyte block, possibly leading to trapped nonequilibrium structures, which are kinetically frozen and do not undergo dissociation to unimers upon dilution [14].

2.3 FROM KINETICALLY FROZEN AGGREGATES TO MACROSURFACTANTS (micelles at thermodynamic equilibrium)

The argument that the topology of the aggregates depends on the preparation route has shown that samples in aqueous solution are not at thermodynamic equilibrium. This feature has been observed in numerous systems of diblocks in aqueous solutions. Many water-soluble block copolymers, for example, poly(styrene)-*b*-poly(acrylic acid) or PS-*b*-PAA and poly(*tert*-butylstyrene)-*b*-poly(styrene sulfonate) or PtBS-*b*-PSS, form frozen aggregates in solution [15,16]. The high glass transition temperature T_g of the insoluble block of PS or PtBS has often been inferred to explain the irreversibility of the self-assembly in solution. However, experiments with a sample of poly(n-butyl acrylate)-*b*-poly(acrylic acid) or PBA-*b*-PAA, whose insoluble blocks (PBA) have a T_g as low as – 55 °C, have shown that such samples form also irreversible aggregates in solution [17, 18]. These results proved that the hydrophobicity of the insoluble block is a major factor favoring a slow association dynamics in solution. Measurements of the interfacial tension between the insoluble block of PBA and the solvent have yielded quantitative evidence that the interfacial tension can induce a potential barrier to free chain – aggregate exchange that is large enough to explain the presence of kinetically frozen aggregates [19]. It has appeared interesting to modify the hydrophobicity of blocks in order to reduce interfacial tension between the insoluble core of aggregates and the water solvent and change the aggregation properties in water in order to come closer to reversibility. Following this idea, a new family of charged water-soluble amphiphilic diblock copolymer, poly(diethyleneglycol ethylether acrylate)-*b*-poly(acrylic acid), or PDEGA-*b*-PAA, has been synthesized and studied, recently. The work has shown, that PDEGA-*b*-PAA system is an example of a synthetic charged amphiphilic diblock copolymer system forming reversible micelles in aqueous solution, and experimentally proved that a key parameter to get reversible self-assembly in diblock systems is a low interfacial tension between the hydrophobic block and the solvent [20].

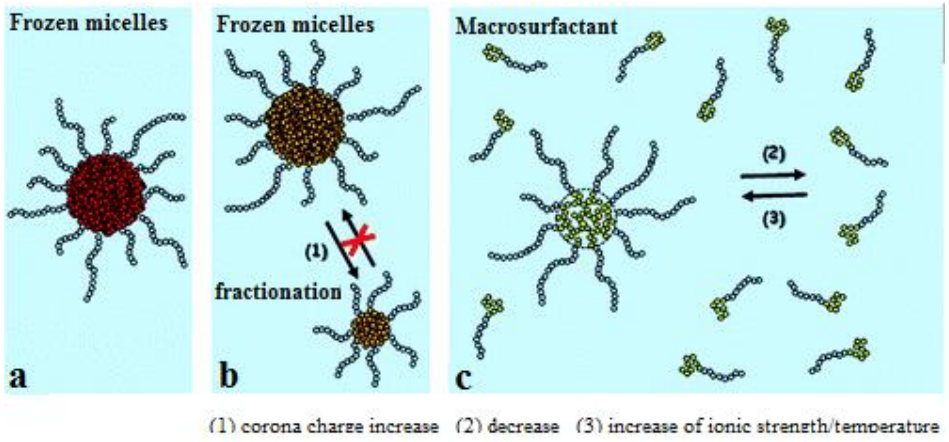

Figure 1. Schematic of the dynamics of micelle reorganization in aqueous solution for decreasing values of the interfacial tension between the core of the micelle and the solution [20].
(a) PS/PAA ($\gamma_{core/water}$ ≈ 35mN/m and T_g(PS) ≈ 100 °C) forms physically and kinetically frozen micelles with no reorganization possible.
(b) PBA-PAA forms a kinetically frozen micelles that can fractionate (1) via an intramicelle and irreversible process.
(c) PDEGA-PAA is a macrosurfactant system with an reversible exchange (2 and 3) between micelles and unimers. Aggregation is favored by higher ionic strength or temperature.

2.4 INTERACTIONS BETWEEN BLOCK COPOLYMERS AND SURFACTANTS

The interaction between polymers and surfactants is described by two critical – concentrations [21-23]. The first is the critical aggregation concentration (cac, sometimes denoted C_1) at which point binding of the surfactant to the polymer first occurs. The cac is generally lower than cmc of the surfactant alone. The second critical concentration (often denoted C_2) is associated with the saturation of the polymer with surfactant aggregates. The cmc of the surfactant (C_m) may also be observed. For some polymer/surfactant systems, C_m and C_2 are coincident. However, in other cases, C_m is less than C_2.

The interactions between various Pluronics and the anionic surfactant SDS has been investigated. It was found that the copolymers form mixed micelles with SDS at concentrations well below the cmc of SDS and that SDS reduces the size

of Pluronic micelles, or can completely suppress micelle formation [24-27]. The formation of mixed micelles, micellar clusters and supramicellar aggregates has been observed in solutions of PS-*b*-PEO diblock with SDS surfactant. The evidence for incorporation of the surfactant into the block copolymer micelles is in the increase in micellar size up to certain concentration [28].

A number of studies have been focused on polyelectrolyte-surfactant complexes, PE-S, formed not only by polyelectrolyte homopolymers, but also by block polyelectrolytes. Most of them deal with double-hydrophilic block copolymers, consisting of a polyelectrolyte block and a neutral hydrophilic block. The formation of polyelectrolyte-surfactant (PE-S) complexes is driven by electrostatic interactions between the surfactant head groups and the polyelectrolyte side groups and hydrophobic interactions between the hydrophobic backbone of the polyelectrolyte and the alkyl chains of the surfactant. It has been reported that, if the stoichiometric ratio between the surfactant molecules and the polyelectrolyte units in the mixture reaches a certain value, the components form self-assembled nanoparticles with core-shell structure similar to amphiphilic copolymer micelles [29]. Copolymers with both type of charged block were studied. Berret and coworkers have performed small-angle scattering (SANS and SAXS) and DLS studies of colloidal complexes resulting from the self-assembly of neutral-*b*-polyelectrolyte diblocks and oppositely charged surfactants. An aggregate with a core-shell structure forms, as sketched in Figure 2.

The core is described as a microphase comprising surfactant micelles linked by the polyelectrolyte blocks. The corona formed by the lengthy neutral chains forms a stabilizing coating and prevention of phase separation. The complexes have hydrodynamic radii in the range 13-58 nm. The cores contain typically a few hundred micelles. The core radius decrease more slowly with core block length than predicted and the neutral block does not have significant influence. The nonequilibrium nature of the self-assembly process was emphasized by the observed dependence of the size of complexes on the initial mixing conditions. Cryo-TEM on the complexes provided direct evidence for internal structure of the micelles, as well as providing dimensions for comparison with indirect scattering techniques [30-33].

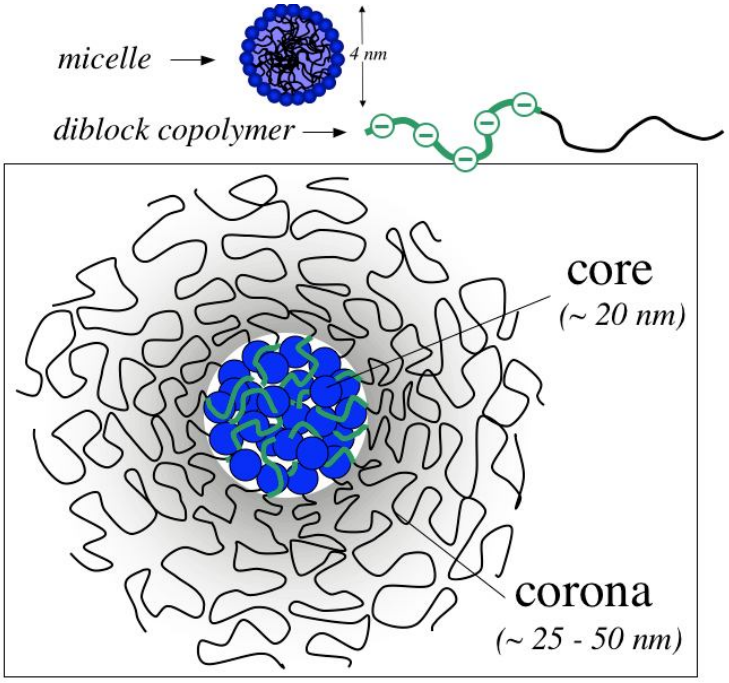

Figure 2. Schematic of core/shell structure formed by complexation between a diblock comprising an anionic poly(sodium acrylate) block and neutral poly(acrylamide) and the cationic surfactant dodecyl trimethylammonium bromide (DTAB) [33].

2.5 CONTROLLED DRUG RELEASE

Block copolymers could be used as carriers for the drugs. Controlled drug delivery technology represents one of the most rapidly advancing areas of science in which chemists and chemical engineers contribute to human health care. Such delivery systems offer numerous advantages compared to conventional dosage forms including efficacy, reduced toxicity, and improved patient compliance and convenience. All controlled release systems aim to improve the effectiveness of drug therapy. This improvement can take the form of increasing therapeutic activity compared to the intensity of side effects, reducing the number of drug administrations required during treatment, or eliminating the need for specialized

drug administration (e.g., repeated injections). Two types of control over drug release can be achieved, temporal and distribution control. In temporal control, drug delivery systems aim to deliver the drug over extended duration or at a specific time during treatment. Controlled release over an extend duration is highly beneficial for drugs that are rapidly metabolized and eliminated from the body after administration. Clinically, temporal control can produce a significant improvement in drug delivery, however maximum possible benefit could be derived from the drug. In distribution control, drug delivery systems aim to target the release of the drug to the precise site of the activity within body. There are two principle situations in which distribution control can be beneficial. The first is when the natural distribution causes drug molecules to encounter tissues and cause major side effects that prohibit further treatment. The second situation is when the natural distribution of the drug does not allow drug molecules to reach their molecular site of action. For example, a drug molecule that acts on a receptor in the brain will not be active if it is distributed by the patient blood system but cannot cross the blood-brain barrier.

A diverse range of the mechanisms have been developed to achieve both temporal and distribution controlled release of drugs using polymers. This diversity is necessary consequence of different drugs imposing various restrictions on the type of delivery system employed. An important consideration in designing polymers for any controlled release mechanism is the fate of the polymer after drug release. Polymers that are naturally excreted from the body are desirable for many controlled release applications. These polymers may be excreted directly via the kidneys or may be biodegraded into smaller molecules that are then excreted. Nondegradable polymers are acceptable in applications in which the delivery system can be recovered after drug release (e.g., removal of patch or insert) or for oral applications in which the polymer passes through the gastrointestinal tract.

Most drug molecules need to be dissolved in the aqueous environment of the patient and freely diffuse within that media before they can act their target receptors. Polymeric devices that achieve temporal controlled release protect drug molecules from this aqueous environment for preprogrammed periods of time. This protection can involve delaying the dissolution of drug molecules, inhibiting the diffusion of the drug out of the device, or controlling the flow of drug solution. Another form of temporal controlled release is responsive drug delivery in which

drug is released in a pulsatile manner only when required the body. In this case, responsive drug delivery systems consist of two components: a sensor that detects the environmental parameter that stimulates drug release and a delivery device that releases drug. For example it was investigated that formation and self-assembly of polymer-surfactant complexes from weak polyelectrolytes reveal strong pH dependency and it makes it possible to design sophisticated pH-sensitive systems undergoing structure transition and releasing biologically-active components upon change in pH in the body [34].

The simplest method of achieving distribution control is to implant the drug delivery system directly at the site, which is suitable only if the site drug action is accessible without risk to the patient and the drug is unable to leave this site. For the majority of diseases that require distribution controlled release of drug, a targeting mechanism must be employed that allows the delivery system to find the desired target. Polymers are used in two types of delivery systems for these applications, colloidal carriers and polymer-drug conjugates. In colloidal formulations, the polymer encapsulates drug within micro- or nanoparticles. In polymer-drug conjugates, the drug is covalently coupled to the polymer. In these forms of distribution controlled release, the polymer acts as a carrier but is not responsible for targeting the delivery device. Biological molecules such as immunoglobulins and carbohydrates are utilized as targeting moieties, or polymer-drug conjugates contain a spacer molecule that is site-specifically cleaved. There are several examples of targeting in which distribution control is an inherent property of the polymeric carrier.

Classification of polymers in controlled release applications can be difficult due to the inherent diversity of structure. However, it is beneficial to attempt this classification because it can highlight common properties within groups of polymers. In broad terms, polymers can be classified as either biodegradable or nonbiodegradable. Biodegradable systems have garnered much of the recent attention and development in drug delivery systems because nonbiodegradable systems need retrieval or further manipulation after introduction into the body.

2.5.1 Poly(ethylene oxide) in controlled drug release

Poly(ethylene oxide) is commonly used to improve the stability and biological performance of colloidal drug carriers. The grafting of PEO to the surface of colloidal carrier has been clearly shown to extend the circulation lifetime of the vehicle in the body, because the PEO corona prevents capturing of the vehicle by the cells of reticuloendothelial system (RES). One of the most noted advantages of PEO is a biocompatibility, because for micellar drug carriers the biocompatibility is of essential importance. PEO is nontoxic and nonimmunogenic. In order to gain an understanding of mechanism by which the presence of PEO increases the circulation longevity of drug carriers it should be considered the physical and chemical properties of the polymer. PEO is a neutral, crystalline polymer with a high solubility in both water and organic solvents. At room temperature, its water solubility is said to be unlimited for all degrees of polymerization. The unique high degree of water solubility of PEO is believed to be due to its "good structural fit with water". The structure of water in the liquid state is believed to approximate its solid state structure which consists of a tetrahedral lattice of hydrogen bonded molecules. It has been suggested that PEO actually fits into the tetrahedral lattice of water facilitating hydrogen bonding between the water molecules and the ether oxygens of PEO. One of the emerging uses for inclusion of PEO in a controlled release system arises from its protein resistivity. The hydrophilic nature of PEO is such that water hydrogen bonds tightly with the polymer chain and thus excludes, or inhibits, protein adsorption. Many research groups are investigating attachment of PEO chains to therapeutic proteins; PEO chains at the surface allow for longer circulation of the protein in the body by prolonging biological events such as endocytosis, phagocytosis, liver uptake and clearance, and other adsorptive processes [35, 36].

2.6 FUNDAMENTALS OF CHARACTERIZATION METHODS

2.6.1 Static light scattering (SLS)

Static light scattering involves measuring the intensity of elastically scattered light as a function of scattering angle. Particles, which are small compared with the wavelength of the light, act as point scatterers, hence the scattered intensity does not depend on scattering angle θ (when corrected for geometrical effects). For larger particles, such as macromolecules, there are variations in the phase of the scattered light from different parts in the macromolecule, which can lead to the destructive or constructive interference of the scattered light in certain directions and to angular dependence of the intensity of scattered light. SLS measurements provide values of the Rayleigh ratio that can be expressed as:

$$R(q) = \frac{I(q)}{I_0} r^2 = \frac{4\pi^2 \alpha_p^2}{\lambda^4 N_A}, \quad (1)$$

where r is the distance from the scattering sample to the detector, $I(q)$ is the time averaged intensity of the scattering light as a function of the scattering vector, q, defined as:

$$q = \frac{4\pi n_0}{\lambda} \sin\frac{\theta}{2}. \quad (2)$$

I_0, is the intensity of the incident light, λ is the wavelength of the used light in vacuum, N_A is the Avogadro constant and α_p is the polarizability of the molecules. Equation (1) shows that the scattered intensity depends strongly on the wavelength of the light and on the polarizability of the scattering centers. The scattering from a solution is observed due to fluctuations of the polarizability, or as expressed macroscopically, fluctuations of the refractive index. In a solution, two sources of such fluctuations can be recognized: density and concentration fluctuations.

Measurement of the scattering intensity at many angles allows for calculation of the root mean square radius, also called the radius of gyration R_g. By measuring the scattering intensity for many samples of various concentrations, the second osmotic virial coefficient A_2, can be calculated. It gives information about the interactions of the macromolecules in solution and so about the excluded volume of one macromolecule for another, which in turn relates to the effective volume fraction of macromolecules in solution. The intensity of scattered light is proportional to the product of the weight-average molecular weight and the concentration of the macromolecule.

The usual procedure for obtaining M_W and A_2 involves Debye plots. At small angles, the inverse scattered intensity is given by:

$$\frac{Kc}{R(q)} = \frac{1}{M_W} + 2A_2c + \ldots \quad , \tag{3}$$

where c is the concentration of polymer, K is an optical constant depending on refractive index, wavelength and polarization of the light:

$$K = \left(4\pi^2 / N_A\lambda^4\right)\left(n_S^2 / R_S\right)\left(\mathrm{d}n/\mathrm{d}c\right)^2 \quad . \tag{4}$$

Here λ is the wavelength of the light, n_S and R_S are refractive index and Rayleigh ratio, respectively, of the solvent background and dn/dc is the refractive index increment. The equation (3) is valid for particles with a diameter smaller then λ/20. Since scattering from larger particles depends on the scattering angle, θ, it is necessary to define an angular scattering function (particle form factor), $P(q)$, which can be written for the low values of θ as a power series:

$$P(q) = 1 - \frac{1}{3}q^2\left\langle R_g^2\right\rangle + \ldots \quad , \tag{5}$$

where $\left\langle R_g^2\right\rangle$ is the z-average radius of gyration and q is scattering vector. The SLS data can be evaluated in several a different ways (Zimm, Berry or Guinier plot)

depending on the size of the particle.

Static light scattering measurements of this work were treated by the Guinier method using the equation:

$$\ln\frac{I(q)}{I(0)} = 1 - \frac{1}{3}R_g^2 q^2 . \tag{6}$$

2.6.2 Dynamic light scattering (DLS)

Dynamic light scattering (DLS), also known as photon correlation spectroscopy (PCS) or quasi-elastic light scattering (QELS), consists in measuring the temporal fluctuations of the intensity of scattered light. The number of photons entering a detector are recorded and analyzed by a digital correlator. The correlation between counts measured at angle θ over an interval t is computed:

$$g^{(2)}(\theta,t) = \lim_{S\to 0}\left[\frac{1}{S}\int_0^S I_\theta(s)\, I_\theta(s+t)\,\mathrm{d}s\right]. \tag{7}$$

The measured intensity correlation function is related to the electric field autocorrelation function, $g^{(1)}(t)$, by the Siegert relation, $g^{(2)}(t)=1+\beta|g^{(1)}(t)|^2$. Laplace transformation of Equation (7) (often using the CONTIN program) yields the distribution of relaxation times, $A(\tau)$:

$$g^{(1)}(t) = \int_0^\infty A(\tau)\exp\left(-\frac{t}{\tau}\right)\mathrm{d}\tau \,. \tag{8}$$

The $A(\tau)$ distributions can be recalculated to the distributions of apparent hydrodynamic radii, R_H^{app}, using the relationship:

$$R_H^{app} = \frac{8\pi n_0^2 k_B T}{3\eta_0 \lambda^2}\sin^2\left(\frac{\theta}{2}\right)\tau , \tag{9}$$

where k_B is the Boltzmann constant, T is the temperature, n_0 is the refractive index of the solvent and η_0 is the viscosity of the solvent.

Autocorrelation functions providing monomodal relaxation time distributions by the CONTIN method can be fitted to the cumulant expansion:

$$\ln g^{(1)}(t,q) = -\Gamma_1(q)t + \frac{\Gamma_2(q)}{2}t^2 + \ldots + \frac{(-1)^n \Gamma_n(q)}{n!}t^n = \sum_{k=1}^{n} \frac{(-1)^k}{k!}\Gamma_k(q)t^k , \tag{10}$$

where $\Gamma_1(q)$ and $\Gamma_2(q)$, respectively, are the first and the second moment of the distribution function of relaxation rates. The diffusion coefficient of the particles, D, can be evaluated by extrapolation of $\Gamma_1(q)/q^2$ using the equation:

$$\frac{\Gamma_1(q)}{q^2} = D\left(1 + CR_g^2 q^2\right), \tag{11}$$

where C is the structural parameter reflecting the shape, polydispersity, and internal dynamics of the scattering particles. Hydrodynamic radius, R_H, can be calculated from D using the Stokes-Einstein formula:

$$R_H = \frac{k_B T}{6\pi\eta D}. \tag{12}$$

2.6.3 Electrophoretic light scattering

Electrophoretic light scattering is the method most popularly used to determine the velocity of the particles suspended in a fluid medium under an applied electric field. In order to determine the speed of the particles' movement, the particles are irradiated with a laser light and the scattered light emitted from the particles is detected. Since the frequency of the scattered light is shifted from the incident light in proportion to the speed of the particles' movement, the electrophoretic mobility of the particles can be measured from the frequency shift (Doppler shift) of the scattered light.

When an electric field is applied to charged particles in the suspension, particles move toward an electrode opposite to their surface charge. Since the velocity is proportional to the amount of charge of the particles, zeta potential can be estimated by measuring the velocity of the particles.

2.6.4 Transmission electron microscopy (TEM)

TEM relies on electron density contrast within a thin film of a sample to provide an image due to spatial variations in transmission of the electron beam. It is possible to use the bright or dark field mode. The bright field mode is the most common mode of operation for a TEM, the contrast of the image comes from the absorption and occlusion of the electrons in the sample: parts of the sample with high electron density or larger thickness occur on image as a dark stains. In the dark field mode, the scattered electrons are detected so a region without the sample will appear dark on the image. In the case of block copolymer solution, the sample is usually prepared by coating directly onto a carbon-coated TEM grid (by spin or dip coating).

2.6.5 Cryogenic field-emission scanning electron microscopy (Cryo-FESEM)

Cryo-FESEM is a technique where scanning electron microscopy (TEM) is used to image cryogenically cooled samples. Rapid cooling into cryogenic liquids is intended to "trap" structures formed in solution, by vitrifying the sample and avoiding crystalization in the solvent.

2.6.6 Nuclear magnetic resonance spectroscopy (NMR)

Nuclear magnetic resonance (^{1}H NMR) has been widely used to probe micelle structure. Proton NMR on copolymers in D_2O is employed to monitor the presence or absence of micellization.

3 EXPERIMENTAL PART

3.1 MATERIALS

3.1.1 Studied block copolymers

The synthesis of three different series of double hydrophilic block copolymers (DHBCs), consisting of poly(ethylene oxide) as the neutral water soluble block and a second polyelectrolyte block of variable chemistry, was accomplished by post polymerization reaction of precursor amphiphilic block copolymers. In particular the synthesis of the precursor PtBOS-PEO was realized by sequential anionic polymerization of tert-butoxystyrene and ethylene oxide utilizing high vacuum techniques, followed by acidic hydrolysis of the poly(tert-butoxystyrene) block to remove the protective *t*-butyl group. The reaction was performed in acetone, a good solvent for PtBOS, PHOS and PEO blocks. PHOS block was subsequently transformed by aminomethylation for the introduction of two dimethyl-aminomethylene groups on each phenolic moiety, giving the NPHOS-PEO block copolymer, which can be considered as high charge density annealed cationic polyelectrolyte when amino groups are protonated, that is, in acidic aqueous solution. Finally, the NPHOS-PEO block copolymers were treated with methyl iodide in THF. The final copolymer (QNPHOS-PEO) contains a block with quaternized amino groups and can be considered as a quenched cationic polyelectrolyte block with two cationic groups in nearly every monomeric unit. The molecular characteristics of synthesized copolymers are presented in Table 1. (The molecular characteristics of the functionalized polymers have been calculated based on the characteristics of the precursor polymer assuming 100% functionalization). Details on the synthesis and characterization of the sample are in ref. [37].

Table 1. Molecular Characteristics of the
Studied Double Hydrophilic Block Copolymers

Sample	M_w x 10^{-3}	M_w/M_n	% wt PEO
PHOS-PEO-4	21.1	1.13	41
NPHOS-PEO-9	52.9	1.09	28
QNPHOS-PEO-4	62.7	1.13	14

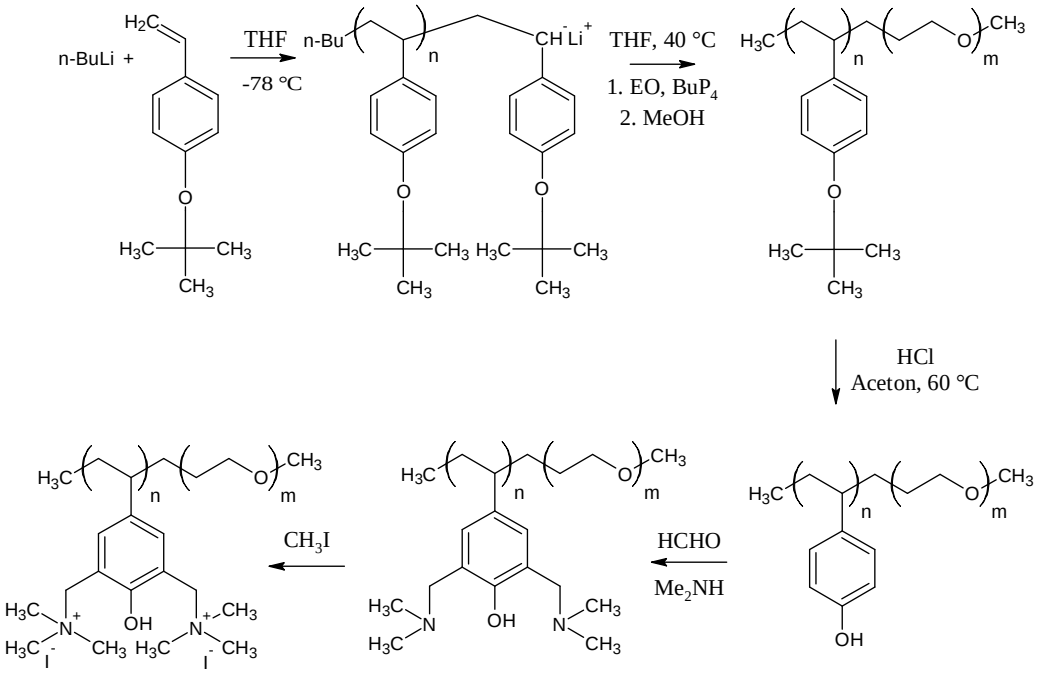

Figure 3. Synthetic scheme for the preparation of the functional DHBCs.

3.1.2 Preparation of nanoparticles

Preparation of PHOS-PEO nanoparticles in alkaline aqueous solution. Samples of PHOS-PEO could not form micelles directly in water, or aqueous NaOH, because of insolubility of the copolymer, however, PHOS-PEO micellizes when dissolved

in mixtures with an organic cosolvent which alone is a good solvent for the hydrophobic block. Tetrahydrofuran (THF) or mixture of THF with various amounts of aqueous 10 mM NaOH (THF/aq. NaOH) were used as initial solvents for PHOS-PEO. 20 mg of the copolymer were dissolved in 3 mL of THF or THF/aq. NaOH solutions and added dropwise to 17 mL of 10mM aqueous NaOH subsequently, so that the final concentration of the PHOS-PEO was 1 mg/mL. The solution was dialyzed stepwise against 10 mM aqueous NaOH (or 10mM NaOD in D_2O for ^1H NMR measurements) to remove THF. To find the optimum composition of the mixed solvent for preparation of well-defined PEO-PHOS nanoparticles in aqueous NaOH, the composition of THF/aq. NaOH was varied from pure THF to 75 vol. % of aqueous 10mM NaOH.

Preparation of NPHOS-PEO nanoparticles in acidic aqueous solution. NPHOS-PEO was dissolved in 0,1M HCl. The concentration of copolymer was 1 mg/mL. Solutions of NPHOS-PEO and SDS (Sigma) were mixed under stirring and left to stand about 24 hours for equilibration prior to measurements. For measurements with a surplus of surfactant copolymer was diluted in 0,1M HCl and in the pure THF, respectively. The concentration of solutions was 10 mg/mL. 0.1 mL of solutions was under stirring dropwise added to 1 mL of 0,1M SDS. The sample with the THF as a solvent was finally dialyzed against distilled water.

3.2 EXPERIMENTAL SET-UP

Static and dynamic light scattering (SLS, DLS). The light scattering measurements were performed on a ALV instrument (ALV, Langen, Germany) consisting of a 22 mW He-Ne laser, operating at the wavelength λ = 632.8 nm, an ALV CGS/8F goniometer, an ALV High QE APD detector and an ALV 5000/EPP multibit, multitau autocorrelator. The measurements were carried out at 25^{o}C and the scattering angles, θ, were ranging from 30° to 150°. The solutions for measurements were filtered through 0.45 μm Acrodisc filters.

Electrophoretic light scattering. ζ-Potential measurements were carried out with a Nano-ZS Zetasizer (Malvern Instruments, U.K.). ζ-Potential values were calculated from electrophoretic mobilities (average of three subsequent

measurements, each of which consisted of 15–100 runs) using the Henry equation in the Smoluchowski approximation, $\mu = \varepsilon\zeta/\eta$, where μ is the electrophoretic mobility and ε is the dielectric constant of the solvent.

Transmission electron microscopy (TEM). TEM micrographs were obtained with a Tecnai G2 Spirit Twin 12 microscope (FEI, Czech Republic). A small amount of the aqueous solution of nanoparticles (2 μL, *c* = 1mg/mL) was sputtered onto a TEM copper grid covered with thin holey carbon film, the liquid was gently removed with filter paper and the rest of the solution was left to evaporate at the room temperature. The dried sample was observed in the TEM microscope at 120 kV using bright field imaging.

Cryogenic field-emission scanning electron microscopy (Cryo-FESEM). A JSM 7401F high resolution scanning electron microscope (JEOL, Ltd., Japan) equipped with an Alto 2500 cryo-attachment (Gatan, Inc., CA) was used for the observation of the frozen aqueous solution of PHOS-PEO nanoparticles. A drop of the solution (5 μL, *c* = 1 mg/mL) was placed on top of the aluminum pin, then the pin was plunged into liquid nitrogen and immediately transferred under vacuum into the chamber of the cryo-attachment. The upper part of the frozen droplet was broken off. The revealed surface was sputter-coated with platinum/palladium at –140°C for 2 min. Thus prepared sample was observed in FESEM operated at the accelerating voltage 1 kV, the beam current of 20 μA, the working distance 8 mm and the stage temperature –135 °C.

Nuclear magnetic resonance spectroscopy (NMR). ^{1}H NMR spectra were recorded on a Varian 300 spectrometer at 25 °C using deuterated tetrahydrofuran (THF-d_8) and 10 mM NaOD in deuterium oxide as solvents. For solutions in THF-d_8 and in 10 mM NaOD in D_2O, solvent residual signals at 3.58 ppm (CH_2O in THF) and 4.80 ppm, respectively, were used as references. Solutions in mixtures of THF-d_8 with 10 mM NaOD in D_2O were referenced to sodium acetate (1.90 ppm) as an internal standard. Copolymer concentrations were 10 mg/mL in solutions containing THF-d_8 and 1 mg/mL for the solution in 10 mM NaOD in D_2O.

Potentiometric titration. The pH measurements were performed with a Radiometer PHM 93 reference pH meter equipped with a PHC 3006 combined glass microelectrode. The pH of the samples was adjusted by adding phosphoric acid.

4 RESULTS AND DISCUSSION

4.1 POLY(4-HYDROXYSTYRENE)-*b*-POLY(ETHYLENE OXIDE)

Results presented in this part are mostly based on a publication [38] of my supervisor, in which I am the second author and my contribution was focused mostly on preparation of the samples and implementation and evaluation of light scattering measurements.

4.1.1 PHOS-PEO association behavior in THF/aq. NaOH

Prior to the preparation of the nanoparticles, solutions of the copolymer in THF/aq. NaOH mixtures were examined using dynamic light scattering to study the PHOS-PEO association behavior. It was prepared the solutions of the copolymer with concentration 20 mg/mL in pure THF and 90, 75, 60, 50 and 40 vol. % THF in aq.NaOH and solutions with concentration 2 mg/mL in 25 vol. % THF in aq.NaOH. Figure 4 illustrates the intensity distribution of apparent hydrodynamic radii of PHOS-PEO aggregates in these solutions, measured by light scattering at $\theta = 90°$. The mean apparent hydrodynamic radii of the most intensive relaxation mode are plotted in Figure 5 (curve 1) together with the scattering intensity at $\theta = 90°$ per the unit PHOS-PEO concentration (curve 2). In pure THF, the R_H distribution is clearly bimodal, indicating the coexistence of individual PHOS-PEO chains (fast diffusion), with the hydrodynamic radius of ca. 5 nm, and large PHOS-PEO aggregates (slow mode). It should be pointed out that DLS measurements provide only apparent R_H values and do not give information about the true shape of the aggregates. Because the aggregates scatter much more strongly than individual PHOS-PEO macromolecules and distributions are weighted by scattering intensity, their concentration is actually lower, than it seems from the highs of peaks in the Figure 4.

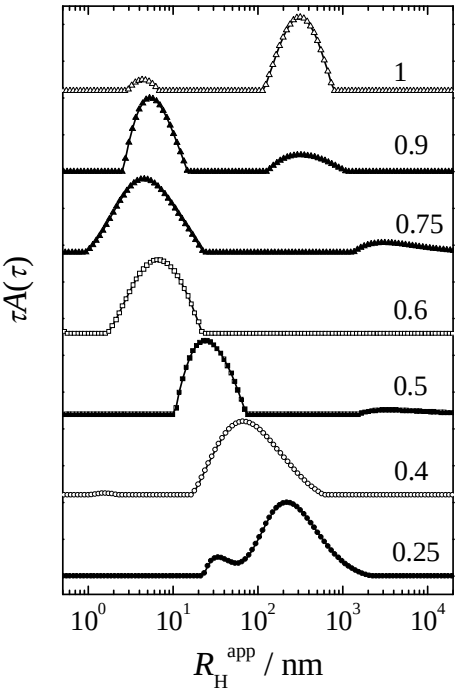

Figure 4. DLS distribution of apparent hydrodynamic radii for PHOS-PEO solutions in THF/10 mM aqueous NaOH mixtures. Numbers above the curves indicate volume fractions of THF, φ_{THF}.

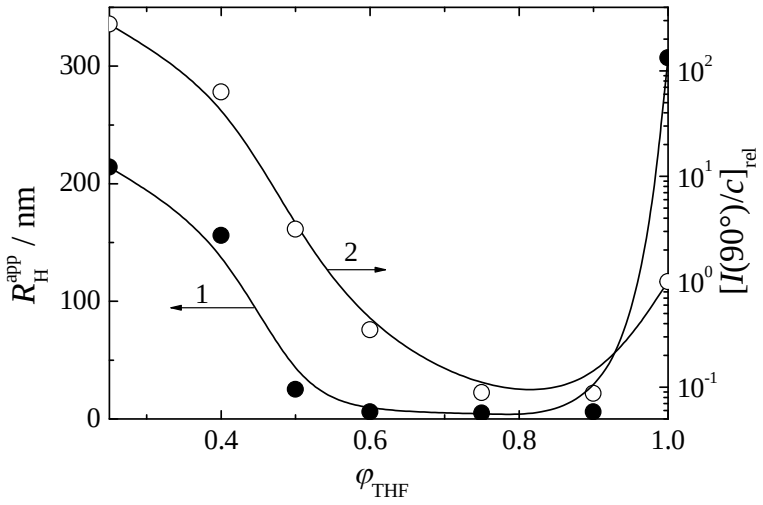

Figure 5. Apparent hydrodynamic radius, R_H^{app} (curve 1), and scattering intensity *per* unit PHOS-PEO concentration at $\theta = 90°$, relative to the value for the solution in pure THF, $[I(90°)/c]_{rel}$ (curve 2), for PHOS-PEO solutions in THF / 10 mM aqueous NaOH mixtures, as functions of THF volume fraction, φ_{THF}.

The presence of aggregates in aqueous polymeric solutions is not uncommon and has been reported for both neutral polymers [39,40] and polyelectrolytes [41,42]. The possible causes of aggregation that have been given in the literature include for example impurities in solvent [43], possible crystallization [44], interchain physical cross-links due to intense hydrogen bonding, chain ends effect [39], etc. Since PHOS-PEO have the capability to form hydrogen bonds both between the −OH groups of PHOS units and between the PHOS –OH group and the oxygen atom of the PEO unit, the formation of the large aggregates is not surprising. The aggregates are loose (as indicated by weak scattering intensity) and disappear after adding alkaline water, most probably due to electrostatic repulsion of ionized PHOS blocks. If the amount of THF is further decreased, the peak of the aggregates shifts toward higher values, because the PHOS-PEO association number increases as a result of prevailing strong attractive hydrophobic interactions between PHOS blocks. The formation of aggregates is accompanied by a strong increase of scattering intensity, which shows that the aggregates in water-rich mixtures have much larger molar mass than those found in THF-rich solutions, which can be explained by the formation of compact PHOS domains, whose faster motion in the PHOS-PEO aggregates is observed in the solution with 25 vol. % THF as an additional relaxation mode in the DLS distribution. The copolymer cannot be dissolved in THF/aq. NaOH mixtures containing less than 25 vol. % THF.

^{1}H NMR spectra of PHOS-PEO shown in Figure 6 were measured in mixtures of THF-d_8 and 10 mM NaOD in D_2O at various mixture compositions from pure THF- d_8 to pure 10mM NaOD in D_2O. In pure THF-d_8 and in the mixture containing 75 vol. % THF there are visible signals at 3.56 and 3.66, respectively, corresponding to CH_2O protons of PEO blocks. With decreasing content of THF-d_8, these signals disappear, despite good solubility of PEO in water and THF/water mixtures. This result suggests that mobility of the PEO blocks is influenced by their interaction with the PHOS blocks, most probably via hydrogen bonding between the –OH groups of PHOS and the oxygen atoms of PEO. No signals of the polymer in ^{1}H NMR spectra of PHOS-PEO solutions in mixtures poor on THF prove that none of the blocks is well solvated and suggest that the blocks are not segregated into a compact PHOS core and swollen PEO shell. PEO chains are probably

collapsed and immobile. Instead simple core/shell structure, aggregates of PHOS-PEO probably contain small PHOS domains which are interconnected by PEO blocks.

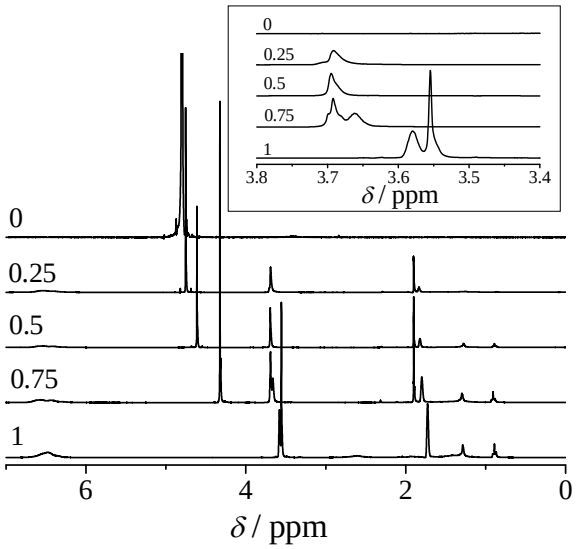

Figure 6. ^{1}H NMR spectra of PHOS-PEO solutions in mixtures of THF-d_8 with 10 mM NaOD in D_2O. Numbers above the curves indicate volume fractions of THF in the mixtures. The spectrum for $\varphi_{THF} = 0$ is 10× magnified. Insert: Detail of the region from 3.4 to 3.8 ppm.

4.1.2 PHOS-PEO nanoparticles in 10mM aqueous NaOH

Nanoparticles prepared in THF/aq. NaOH mixtures of various compound and transferred into aqueous NaOH via stepwise dialysis had different stability depending on the amount of THF. When using PHOS-PEO solutions in THF/aq. NaOH mixtures containing 40 and 50 vol. % THF, the preparation protocol described in the Experimental part provided stable nanoparticle dispersions in 10 mM aqueous NaOH. From other THF/aq. NaOH solvent compositions, highly unstable suspensions of PEO-PHOS nanoparticles undergoing precipitation on the time scale of days were formed after dialyses into NaOH aq media. Therefore, only the aqueous solutions prepared from the PEO-PHOS solutions in 40 and 50 vol. % THF were used for further study (further denoted as PHOS-PEO-I and PHOS-PEO-II, respectively). The narrow range of THF/aq. NaOH mixture compositions providing stable PHOS-PEO nanoparticles in aqueous NaOH can be explained on the basis

of PHOS-PEO association behavior in THF containing solutions: In THF-rich solutions, PHOS-PEO is dissolved as individual polymer chains or large loose aggregates which fail to form the compact hydrogen-bond stabilized particles during the sudden change of the solvent composition which results in precipitation of the copolymer. On the contrary, in solutions with lower content of THF, the formed nanoparticles are too large and tend to coagulate if the content of THF is decreased.

The PHOS-PEO nanoparticles in alkaline solutions were characterized by light scattering measurements. Both static and dynamic measurements were carried out. According to the turbidity of the samples prepared with the concentration of 1 mg/mL, the solutions of the copolymer were diluted 10-times with 10 mM aqueous NaOH prior to the measurements, in order to suppress interparticle interactions and to avoid multiple scattering. Measured SLS data were fitted by Guinier plot. Figure 7 shows Guinier plots for the scattering from 0.1 mg/mL solution of PHOS-PEO-I (curve 1) and PHOS-PEO-II (curve 2) nanoparticles; the scattering curve for PHOS-PEO-II exhibits a minimum in the high q-region at $q_{min} = 24.1\ \mu m^{-1}$.

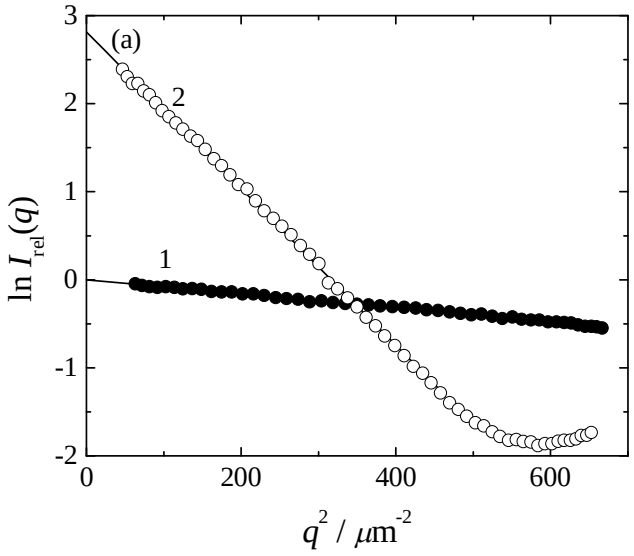

Figure 7. Guinier plot of the scattering curves of the PHOS-PEO nanoparticles, PHOS-PEO-I (curve 1) and PHOS-PEO-II (curve 2).

For the PHOS-PEO-II measurements were implemented also at five different concentrations and the final radius of gyration, $R_{g,}$ value was obtained by extrapolation at a zero concentration (in order to avoid the influence of the second virial coefficient). The concentration of the samples varied from 0.01 mg/mL to 0.625 μg/mL. The extrapolated value of R_g was 118.2 nm (Figure 8).

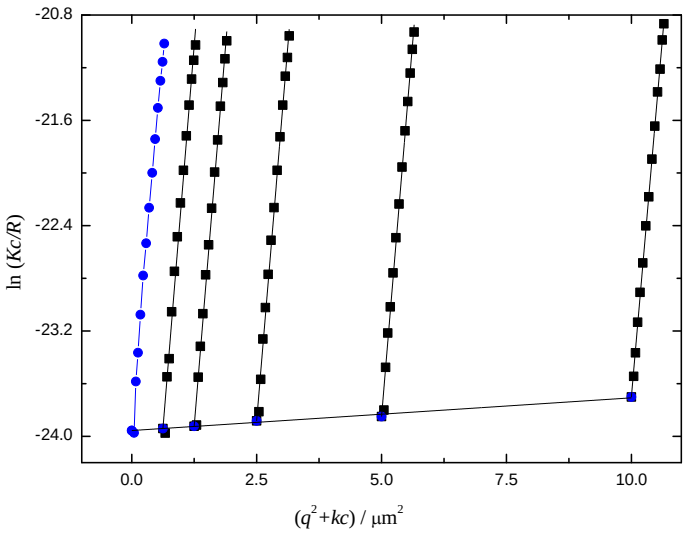

Figure 8. Guinier plot of the scattering curves of the PHOS-PEO-I nanoparticles at various concentration (10; 5; 2.25; 1.125; 0.625 μg/mL).

Results of the evaluation of both static and dynamic LS data are summarized in Table 2.

Table 2. Light Scattering Characteristics of PHOS-PEO Nanoparticles in Alkaline Aqueous Solution

Nanoparticles	R_g, nm	R_H, nm	ρ	$I_{rel}(0)$
PHOS-PEO-I	48	57	0.84	1
PHOS-PEO-II	165	193	0.85	16.6

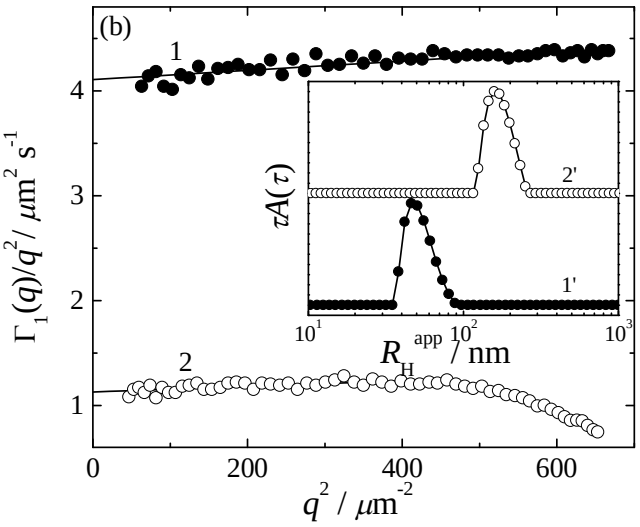

Figure 9. Dynamic Zimm plot of the apparent diffusion coefficients of the PHOS-PEO nanoparticles, PHOS-PEO-I (curve 1) and PHOS-PEO-II (curve 2). Insert shows corresponding DLS distributions of apparent hydrodynamic radii at $\theta = 90°$ for PHOS-PEO-I (curve 1') and PHOS-PEO-II (curve 2').

The gyration-to-hydrodynamic radius ratio, $\rho = R_g/R_H$, for both nanoparticles is close to the value for the hard sphere, $\rho_s = 0.775$. The particle form factor for homogeneous spherical particles is described by the function:

$$P(q,R) = \left(\frac{3\left[\sin(qR) - qR\cos(qR) \right]}{(qR)^3} \right)^2, \tag{15}$$

where R is the radius of the sphere. Equation (15) is an oscillating function with the position of the first minimum at $qR = 4.49$ as shown in Figure 10. It should be noted, that for polydisperse samples these oscillations are not as well pronounced. The minimum of the scattering function of the PHOS-PEO-II at $q_{min} = 24.1$ μm^{-1} is consistent with the spherical shape: Taking the hydrodynamic radius $R_{H,II} = 193$ nm as the radius of the hard sphere, we obtain $q_{min}R_{H,II} = 4.65$ which compares well with the value for the first minimum in the hard sphere form factor, $q_{min}R_s = 4.49$.

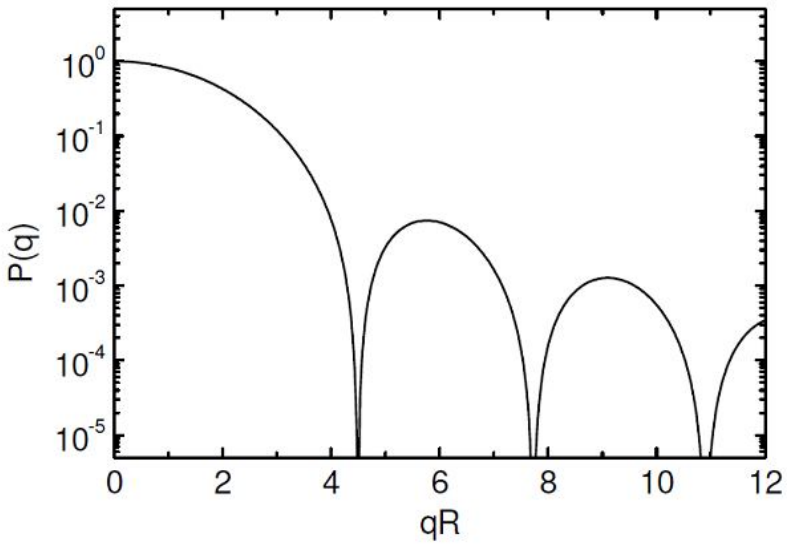

Figure 10. Form factor $P(q)$ for monodisperse spherical particles.

Figure 11 shows the experimental data from SLS measurements of PHOS-PEO-II (the concentration 0.01 mg/mL) fitted to the scattering form factor of monodisperse and polydisperse hard spheres.

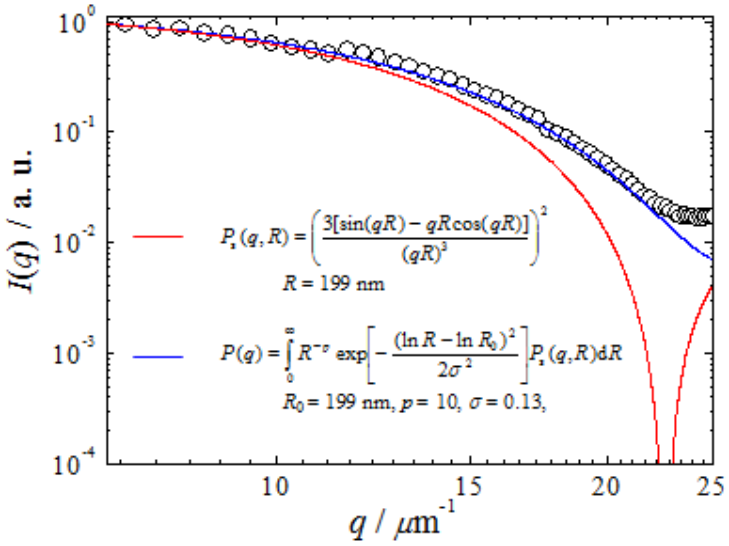

Figure 11. SLS scattering data of PHOS-PEO –II fitted to the scattering form factor of monodisperse and polydisperse hard spheres.

TEM and Cryo-FESEM imaging were accomplished in order to confirm the assumed structure and to determine the shape and real geometric size of the PHOS-PEO nanoparticles from both samples. Nanoparticles were imaged by TEM in dry state and Cryo-FESEM on the fracture surface of frozen amorphous ice of the solution. The micrographs are shown in Figure 12. In the micrographs there are displayed individual spherical particles and also their clusters. It is worth mentioning that PHOS-PEO solutions used for preparation of electron microscopy samples were 10-times more concentrated that those used for light scattering measurements. That is why clusters were not revealed by LS measurements. The detailed look on the micrographs reveals that they are not perfectly homogeneous but contain cavities (or channels): TEM displays the cavities as light spots (indicating a lower electron density), while in FESEM micrographs which maps the surface of the particles, they are visible as holes. The presence of cavities in the nanoparticles, however, is not in contradiction with the proposed structure because they can form as a result of local arrangement of PHOS and PEO chains (formation of small domains) in the nanoparticles. The average radii of the particles (~ 30 nm for sample I, ~ 100 nm for sample II) are in a reasonable agreement to the size obtained from light scattering measurements. The number-averaged values estimated from the electron micrographs are lower, but the difference mostly comes from different weighting procedure. This difference can be eliminated by the conversion of intensity-weighted aggregates distribution function obtained by DLS to mass-weighted or number weighted one, which shifts the distribution maximum to lower R_H values. The average size, spherical shape and size distribution of dried particles in TEM micrographs correspond quite well to the morphology of flash-frozen nanoparticles in cryo-FESEM micrographs (compare Fig. 12a and 12b, 12c and 12d), which also means that the nanoparticles do not collapse upon drying in vacuum conditions.

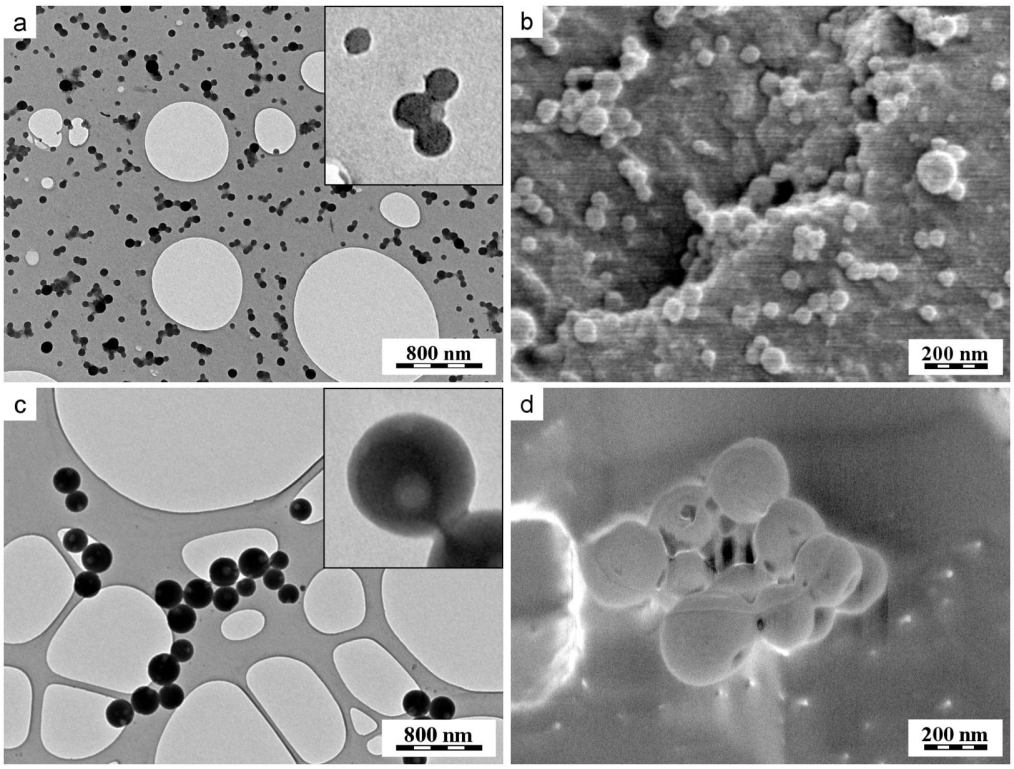

Figure 12. (a,c) TEM and (b,d) Cryo-FESEM micrographs of PHOS-PEO nanoparticles, PHOS-PEO-I (a,b) and PHOS-PEO-II (c,d). Inserts in (a) and (c) show detailed views of the nanoparticles; the real width of both inserts is 300 nm.

The dependence of the size of the particles on the preparation procedure (namely, on the composition of the initial THF/aq. NaOH mixture) confirmed the assumption that the particles are kinetically frozen, non-equilibrium structures. It should be pointed out that PHOS-PEO aggregates in the 50% THF solution with the hydrodynamic radius of 25 nm provide almost eight times larger nanoparticles (PHOS-PEO-II) after transfer to 10 mM aqueous NaOH, while in the case of the 40% THF solution, the PHOS-PEO-I nanoparticles are on the contrary about three times smaller than the “parent“ aggregates with the hydrodynamic radius of 150 nm. It suggests that in the latter case the effect of collapse of the copolymer chains dominates over the size increase caused by the aggregation.

The response of the nanoparticles (PHOS-PEO-I) to the solution pH was further studied by static, dynamic, and electrophoretic light scattering. pH of the solution was adjusted with phosphoric acid. The results of the measurements are summarized in Figure 13. Small changes in the hydrodynamic radius in the alkaline region between pH 12 and pH 9 suggest that the nanoparticles are charged only on the surface so that the decreasing electrostatic repulsion between PHOS blocks does not affect the particle size. Aggregation of the particles below pH 9 manifests itself by a strong increase both in the scattering intensity (curve 1) and in their hydrodynamic radius (curve 2). The inset of Figure 13 shows the pH dependence of the ζ-potential of the nanoparticles. The negative surface charge decreases with decreasing pH as a result of protonation of ionized $–O^-$ groups of PHOS. In accordance with the LS measurements, the absolute value of the ζ-potential falls below the critical value of 30 mV at pH < 9, that is, in the same region where the aggregation of the nanoparticles is observed. These results indicate that the nanoparticles are stabilized electrostatically and confirm the assumption that PEO does not form a segregated water-soluble shell which would stabilize the particles in the solution sterically.

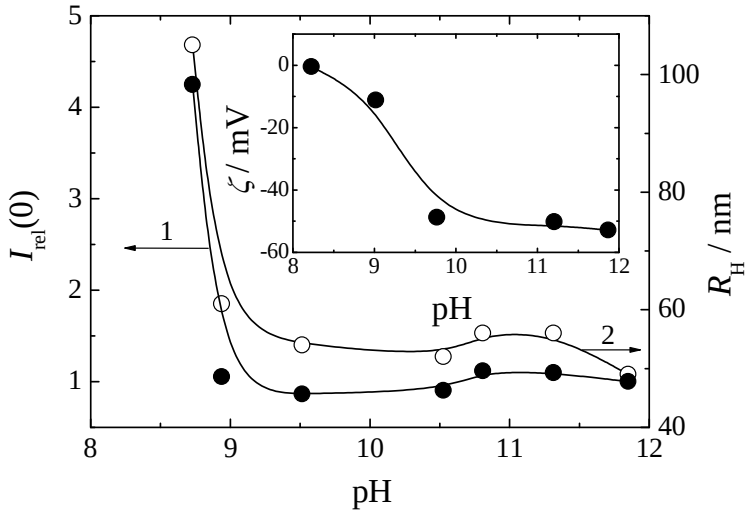

Figure 13. Forward scattering intensity, $I_{rel}(0)$ (curve 1), relatively to the value at pH 11.9, and hydrodynamic radius, R_H (curve 2) of PHOS-PEO nanoparticles (PHOS-PEO-II), in aqueous solution, as functions of pH. Insert: ζ-potential of PHOS-PEO nanoparticles (PHOS-PEO-II) as a function of pH.

4.1.3 Polyelectrolyte-surfactant complexes of PHOS-PEO

The aim of this study was also to investigate the interactions between the copolymer and oppositely charged surfactant. In this study, cationic surfactant DTAB was used, because of the fact that in the solution with pH around 12, PHOS-PEO undergoes ionization of phenolic groups and becomes negatively charged. The measurements were done with the sample of PHOS-PEO-II. The theoretical stoichiometric ratio between the surfactant molecules and the polyelectrolyte units (assumption of the complete ionization of all phenolic groups) varied from $\beta = 0$ to $\beta = 2$. The addition of the surfactant led to the formation of aggregates, which was accompanied by an increase in turbidity observable by a naked eye. Size and structure of the aggregates were studied by a combination of light scattering and TEM. Scattering intensity (relative to the value for stoichiometric ratio $\beta = 0$) and values of the radius of the gyration, R_g, as functions of the stoichiometric ratio, β, are shown in Figure 14. SLS indicates that, R_g of aggregates grows from 150 nm to 300 nm when the DTAB concentration is increased from $\beta = 0$ to $\beta = 2$.

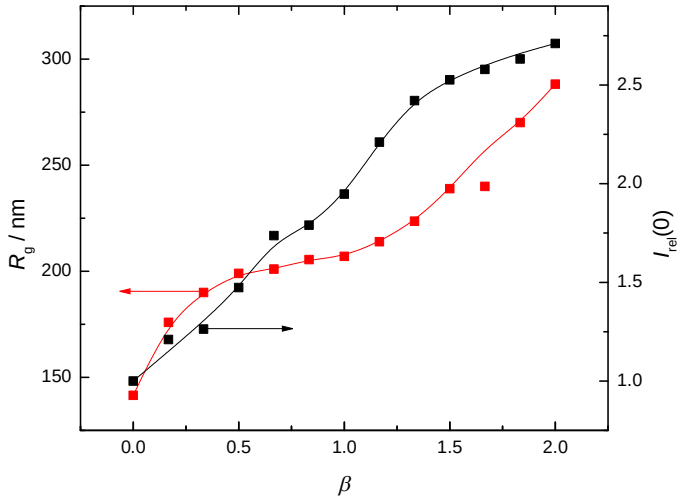

Figure 14. Radius of gyration, R_g, and scattering intensity, $I_{rel}(0)$ (relatively to the value at stoichiometric ratio, $\beta = 0$), of nanoparticles in PHOS-PEO-II/DTAB aqueous solutions as functions of the stoichiometric ratio, β.

Figure 15 shows the micrographs of the solution at β = 0 and β = 1. Compact nanoparticles present in the solution of the pure copolymer, disrupt after addition of the surfactant. This result suggests that molecules of the surfactant compensate the negative charge on the surface of the particles and thus reduce their electrostatical stabilization. Molecules of surfactant can also penetrate into the cavities of the nanoparticles and decrease hydrophobic interactions between PHOS blocks. Unlike other systems of a double hydrophilic block polyelectrolyte and oppositely charged surfactants [30-32], system PHOS-PEO/DTAB does not form core – shell particles around the stoichiometric ratio corresponding to charge equivalence.

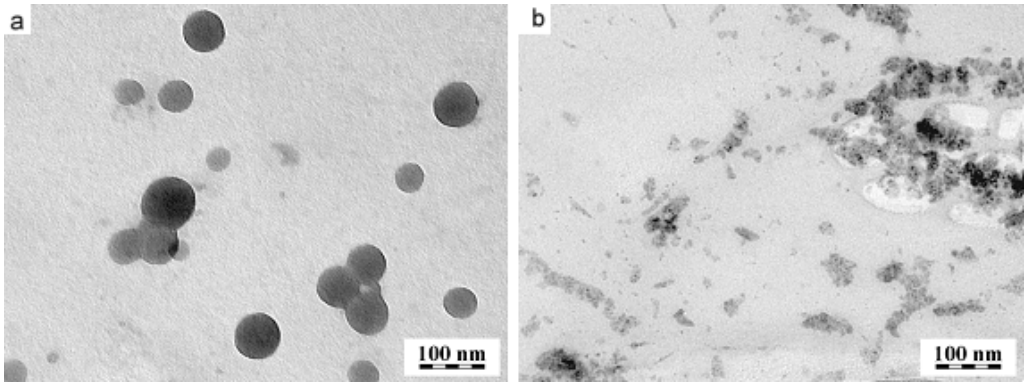

Figure 15. TEM micrographs of (a) PHOS-PEO-II nanoparticles and (b) PHOS-PEO-II/DTAB complexes (stoichiometric ratio, β = 1).

4.2 POLY[3,5-BIS(DIMETHYLAMINOMETHYL)-4-HYDROXYSTYRENE]-*b*-POLY(ETHYLENE OXIDE)

In this chapter, we investigate the formation of polyelectrolyte – surfactant (PE-S) complexes of poly[3,5-bis(dimethylaminomethyl)-4-hydroxystyrene]-*block*-poly-(ethylene oxide) (NPHOS-PEO) and sodium dodecyl sulfate (SDS) in aqueous solution. NPHOS-PEO is directly soluble in acidic aqueous solution and due to the protonation of dimethylamino groups it becomes positively charged. Assuming the complete protonation of all dimethylamino groups, the polyelectrolyte block consists of dicationic monomeric units, so that the surfactant/polymer stoichiometric ratio, β, of SDS/NPHOS monomeric units corresponds to the zero net charge of the complex at β = 2.

The formation of the aggregates was studied mainly by light scattering measurements. Figure 16 shows DLS distribution of hydrodynamic radii of particles formed in SDS/NPHOS-PEO solutions at various stoichiometric ratios, β. The R_H distribution from the pure copolymer solution consists of two modes, which indicates coexistence of two types of particles with different size, probably individual polymer chains and a small amount of aggregates. The addition of surfactant supports the process of aggregation and changes the distribution of R_H from bimodal to monomodal with mean value of hydrodynamic radius around 120 nm. With further addition of the surfactant the maximum of the peak shifts slightly to higher values. At $\beta = \sim 2.5$, some precipitate has appeared in the solution. Because of a small amount of the precipitate at the bottom of the tubes, the solutions were transferred into Eppendorf tubes and centrifuged for a few minutes. Supernatants of these solutions were further used for the scattering measurements and it was found that distribution of hydrodynamic radius again became bimodal, probably due to the formation of large aggregates as the solubility limit approached. Further increase in the stoichiometric ratio ($\beta > 3$) resulted into dissolution of the precipitate, but the distribution of hydrodynamic radius remained bimodal.

Figure 17 illustrates the results of the static light scattering measurements. It shows the dependence of the gyration radius and the relative scattering intensity on the SDS/NPHOS-PEO stoichiometric ratio. A strong increase in the scattering intensity after the very first addition of the surfactant confirms the formation of aggregates. A decrease of gyration radius is most likely connected with charge compensation, which causes a decrease in the electrostatic repulsion between positively charged protonated dimethylamino groups.

It is noteworthy that when the NPHOS block is in neutral state, NPHOS-PEO does not exhibit self-assembly behavior of an amphiphilic diblock copolymer despite the hydrophobicity of the NPHOS backbone. When NPHOS-PEO copolymer is dissolved in THF (a good solvent for both blocks) and the solution is added to a surplus of water, large polydisperse aggregates are formed instead of core-shell micelles with the NPHOS core and the PEO shell (Fig. 18a). This difference in the aggregation behavior can be caused by conformational rigidity of NPHOS chains which prevents the system from corresponding rearrangement. (A similar behavior was observed in the case of QNPHOS-PEO/SDS aggregates [41], see Section 4.3).

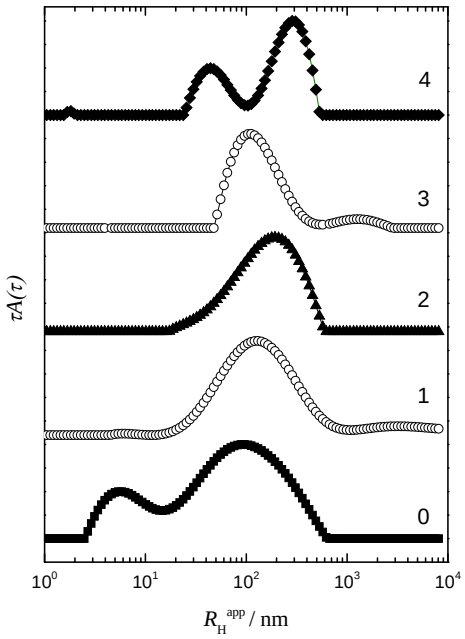

Figure 16. DLS distributions of apparent hydrodynamic radii of the NPHOS-PEO copolymer and NPHOS-PEO/SDS complexes in aqueous solutions. Stoichiometric ratios, β, of the complexes, are indicated above the corresponding curves.

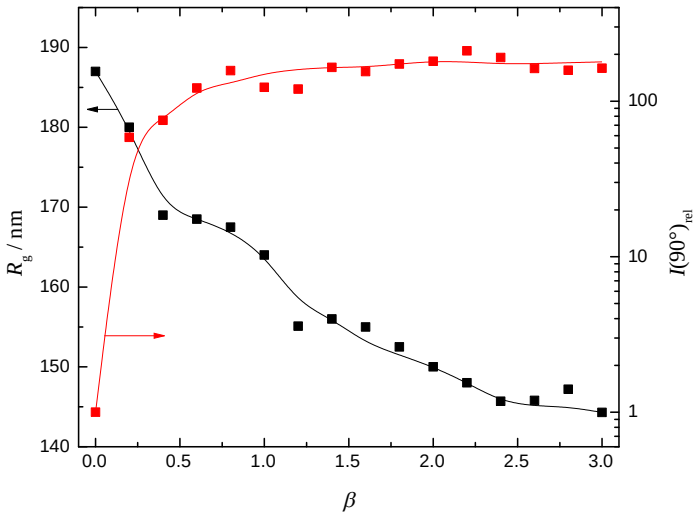

Figure 17. Radius of gyration, R_g, and scattering intensity, $I(90°)_{rel}$ (relatively to the value at stoichiometric ratio, $\beta = 0$), of nanoparticles in SDS/NPHOS-PEO aqueous solutions as functions of the stoichiometric ratio, β.

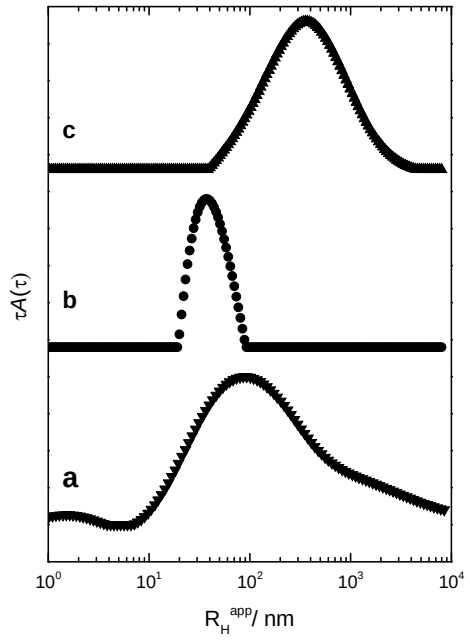

Figure 18. DLS distributions of apparent hydrodynamic radii for NPHOS-PEO diluted in THF and added to the surplus of (a) pure water, (b) 0.1 M aqueous SDS and (c) after the removal of SDS.

Much smaller aggregates with narrower size distributions are formed when NPHOS-PEO solution in THF is added to 0.1 M aqueous solution of SDS instead of pure water (Fig. 18b). Since NPHOS blocks are in neutral state, the interaction of SDS with the copolymer is hydrophobic instead of electrostatic: When the copolymer demix from the solution, SDS adsorbs on the newly formed interface between the hydrophobic polymer microphase and the aqueous phase, decreasing the size of the formed particles and stabilizing them in the solution by decreasing the surface interaction energy. SANS measurements of the small aggregates formed in 0.1 M SDS (data not shown) reveal the $I(q) \propto q^{-4}$ dependence in the q range indicating particles with a sharp boundary instead of core-shell structures with a swollen core. This result suggests that NPHOS-PEO could form spherical particles with intermixed NPHOS and PEO blocks as in the case of PHOS-PEO [38]. The removal of SDS by dialysis leads to attraction of the small particles and to the formation of large polydisperse aggregates similar to those formed after adding the THF solution to pure water (Fig. 18c).

4.3 COMPARISON OF PHOS-*b*-PEO, NPHOS-*b*-PEO AND QNPHOS-*b*-PEO

The goal of this part is to compare the behavior of PHOS-PEO and NPHOS-PEO studied in the frame of my own experimental work and poly[3,5-bis (trimethylammoniummethyl)-4-hydroxystyrene iodide]-*block*-poly(ethylene oxide) (QNPHOS-PEO), which was the subject of earlier studies of my supervisor and other members of our research group [41].

An important difference between these copolymers is their solubility in water. It was reported previously that while PHOS blocks are expected to be water-soluble above pH 9 due to ionization of phenolic groups, PHOS-PEO copolymers dissolve only in strongly alkaline aqueous solutions (pH > 11). For pH values lower than 11, precipitation was observed depending on the copolymer composition, probably due to the formation of hydrogen bonds between PEO and OH groups of the PHOS block. Because of the fact, that direct dissolution of PHOS-PEO is impossible also above pH 11, the aqueous solutions of polymeric nanoparticles must be prepared indirectly by dissolution in a mixture of a good solvent for the hydrophobic block and water. NPHOS-PEO is soluble in acidic aqueous media at pH lower than 8, due to the protonation of the two dimethylamino groups of the NPHOS block. Finally QNPHOS-PEO was found to be directly soluble in aqueous solutions in whole range of pH. The solution behavior of the two first types of classes of DHBCs as a function of pH is complex and depends strongly on copolymer composition [36].

Another interesting property is the self-assembly behavior in aqueous solution without the presence of any surfactant. It was found that PHOS-PEO form compact spherical nanoparticles, which are in alkaline solutions stabilized electrostatically by ionized PHOS units on the surface (Scheme 1). The distribution of apparent hydrodynamic radius is monomodal and quite narrow, which means that the formed aggregates have a low polydispersity. On the contrary, the distributions of apparent hydrodynamic radii of the pure NPHOS-PEO and QNPHOS-PEO are wide and both consist of two modes corresponding presumably to individual polymer chains and aggregates (Figure 19).

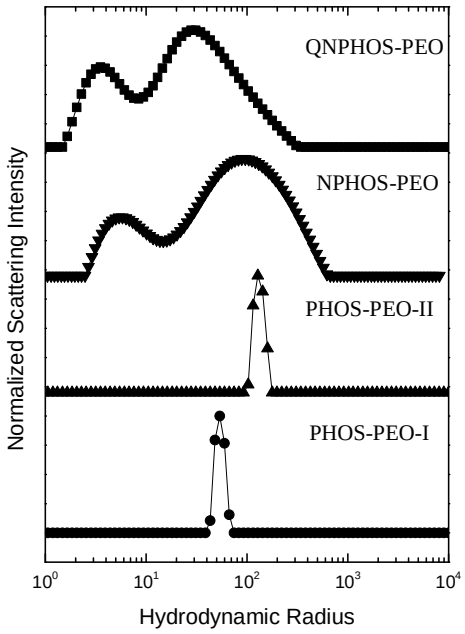

Figure 19. DLS distributions of apparent hydrodynamic radii at $\theta = 90°$ for PHOS-PEO-I, PHOS-PEO-II, NPHOS-PEO and QNPHOS-PEO. Concentration of copolymers 0.1 mg/mL.

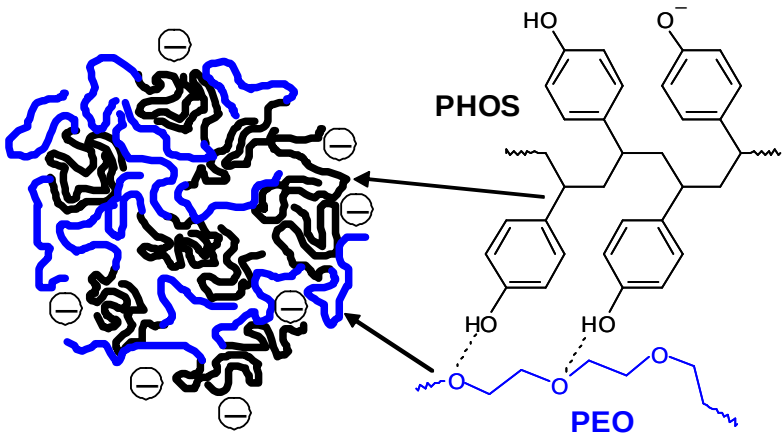

Scheme 1. Structure of the PHOS-PEO nanoparticles in alkaline aqueous solution.

Interactions between copolymers and oppositely charged surfactants were also studied. The results of the measurements have shown, that the structure of the resulting particles is different for each copolymer, but none of them has a core-shell structure, like similar systems described before in literature.

Addition of the surfactant to PHOS-PEO solution causes that well–defined spherical nanoparticles are loosing their compactness due to the disruption hydrophobic interactions between PHOS blocks which contribute to the stabilization.

On the contrary, addition of the surfactant to the solution of NPHOS-PEO initiates aggregation accompanied with increase of the scattering intensity, but formed aggregates become more compact, because their radius of gyration decreases.

Based on light scattering and SAXS measurements, it was found that mixing QNPHOS-PEO copolymer with SDS in aqueous solution leads to the formation of aggregates, which contain densely packed DS micelles interacting with QNPHOS blocks (Scheme 2). SAXS data were fitted assuming contributions from free copolymer chains, PE-S aggregates described by a mass fractal model, and densely packed surfactant micelles inside the aggregates. Inability of the SDS/QNPHOS-PEO system to undergo the transition to core-shell particles stems from strong hydrophobic interactions between QNPHOS blocks and their conformational rigidity. Complex precipitates before the amount of DS anions in the system reaches the number of trimethylammonium groups at QNPHOS blocks as a result of steric hindrances for the surfactant anions because of the high positive charge density at the QNPHOS chains.

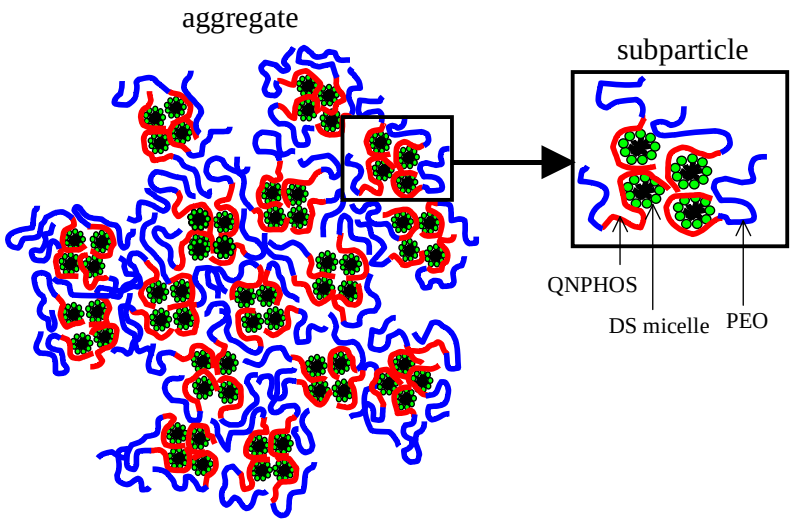

Scheme 2. Morphology of QNPHOS-PEO/SDS aggregates [41].

5 SUMMARY AND GENERAL DISCUSSION

In the presented work self-assembly behavior of double hydrophilic block copolymers based on poly(4-hydroxystyrene) derivatives and poly(ethylene oxide) was investigated. It was found that well-defined compact spherical nanoparticles which are stable in alkaline aqueous solutions down to pH 9 can be prepared by dialysis from solutions of the PHOS-PEO copolymer in mixtures of water and tetrahydrofuran as a cosolvent. Based on the results of elaborated measurements it can be concluded that hydrophilic PEO blocks in the nanoparticles are intermixed with collapsed PHOS blocks due to hydrogen bond interaction and nanoparticles are stabilized electrostatically by ionized PHOS units on the surface. Addition of the oppositely charged surfactant disrupts the compactness of the nanoparticles.

Formation of polyelectrolyte – surfactant complexes of NPHOS-PEO and SDS in aqueous solution was studied by light scattering measurements. The process of aggregation was observed, but to get more information about the structure of the formed aggregates further measurements have to be accomplished.

Mixing the QNPHOS-PEO copolymer with SDS in aqueous solution leads to the formation of aggregates containing densely packed DS micelles interacting with QNPHOS blocks. It was found that, unlike other systems of a double hydrophilic block polyelectrolyte and an oppositely charged surfactant, PE-S aggregates of the QNPHOS-PEO/SDS system precipitate before reaching the charge equivalence.

The obtained results demonstrate that water-soluble nanoparticles based on block copolymers can be formed without segregation of the solvophilic and solvophobic block of the copolymer to a core-shell structure. Studied copolymers exhibit markedly different associative behavior, indicating that specific effects play an important role in the process of aggregation.

References

[1] Meier, M. A. R.; Aerts, S. N. H.; Staal, B. B. P.; Rasa, M.; Schubert, U. S. *Macromol. Rapid Commun.* **2005**, 26, 1918-1924.

[2] Šachl, R.; Uchman, M.; Matějíček, P.; Procházka, K.; Štěpánek, M. *Langmuir* **2007**, 23, 3395-3400.

[3] Ma, Y.; Cao, T.; Webber, S. E. *Macromolecules* **1998**, 31, 1773-1778.

[4] Uchman, M.; Procházka, K.; Štěpánek, M. *Langmuir* **2008**, 24, 12017-12025.

[5] Tuzar, Z.; Kratochvil, P. *Adv. Colloid Interface Sci* **1976**, 6, 201-32.

[6] Zhou, Z.; Chu, B. *J Colloid Interface Sci* **1988**, 126, 171-80.

[7] Nystrom, B.; Kjoniksen, A.L.; *Langmuir* **1997**, 13, 4520-4526.

[8] Price, C. *Pure Appl. Chem.* **1983**, 55 (10), 1563-1572.

[9] Alexandridis, P.; Yang, L. *Macromolecules* **2000**, 33 (9), 3382-3391.

[10] Quintana, J. R.; Villacampa, M.; Katime, I. A. *Macromolecules* **1993**, 26 (4), 601-605.

[11] Quintana, J. R.; Villacampa, M.; Katime, I. A. *Polymer* **1993**, 34 (11), 2380-2385.

[12] Quintana, J. R.; Janez, M. D.; Katime, I. A. *Langmuir* **1997**, 13 (10), 2640-2646.

[13] Quintana, J. R.; Janez, M. D.; Katime, I. A. *Polymer* **1998**, 39 (11), 2111-2117.

[14] Hamley, I. *Block Copolymers in Solution: Fundamentals and Applications* ; John Wiley & Sons Ltd: Chichester, England, 2005.

[15] Amiel, C.; Sikka, M.; Schneider, J. W.; Tsao, Y. H.; Tirrell, M.; Mays, J. W. *Macromolecules* **1995**, 28, 3125-31314.

[16] Kaewsaiha, P.; Matsumoto, K.; Matsuoka, H. *Langmuir* **2005**, 21, 9938-9945.

[17] Colombani, O.; Bukhardt, M.; Drechsler, M.; Ruppel, M.; Schumacher, M.; Gradzielski, M.; Schweins, R.; Müller, A. H. E. *J. Phys. Chem. B* **2009**, 113, 4218-4225.

[18] Colombani, O.; Ruppel, M.; Schumacher, M.; Pergusov, D.; Schubert, F.; Müller, A. H. E. *Macromolecules* **2007**, 316, 897-911.

[19] Jacquin, M. et al. *Journal of Colloid and Interface Science* **2007**, 316, 897-911.

[20] Jacquin, M. et al. *Langmuir* **2010**, 26(24), 18681-18693.

[21] Ghoreishi, S. M.; Li, Y.; Bloor, D. M.; Warr, J.; Wyn-Jones, E. *Langmuir* **1999**, 15, 4380-4387.

[22] Li, Y.; Ghoreishi, S. M.; Warr, J.; Bloor, D. M.; Holzwarth, J. F.; Wyn-Jones, E. *Langmuir* **1999**, 15, 6326-6332.

[23] Dai, S.; Tam, K. C.; Li, L. *Macromolecules* **2001**, 34, 7049-7055.

[24] Li, Y.; Xu, R.; Bloor, D. M.; Holzwarth, J. F.; Wyn-Jones, E. *Langmuir* **2000**, 16 (26), 10515-10520.

[25] Thurn, T.; Couderc, S.; Sidhu,; Bloor, D.M.; Penfold, J.; Holzwarth, J. F.; Wyn-Jones, E. *Langmuir* **2002**, 18 (24), 9267-9275.

[26] Zhang, K.; Lindman, B.; Coppola, L. *Langmuir* **1995**, 11 (2), 538-542.

[27] Hecht, E.; Hoffmann, H. *Langmuir* **1994**, 10 (1), 86-91.

[28] Bronstein L.M., Chernyshov D.M., Vorontsov E., Timofeeva G.I., Dubrovina L.V.,Valetsky P.M., Kazakov S., Khokhlov A.R. *J. Phys. Chem. B* **2001**, 105(38), 9077-9082.

[29] Bronich, T.K.; Kabanov, A.V.; Kabanov, V.A.; Yu, K.; Eisenberg, A. *Macromolecules* **1997**, 30, 3519-3525.

[30] Berret, J.F.; Cristobal, G.; Herve, P.; Oberdisse, J.; Grillo, I. *Eur. Phys. J. E* **2002**, 9, 301-311.

[31] Berret, J.F.; Herve, P.; Aguerre-Chariol, O.; Oberdisse, J. *J. Phys. Chem. B* **2003**, 107, 8111-8118.

[32] Berret, J.F.; Vigolo, B.; Eng, R.; Herev, P.; Grillo, I.; Yang, I. *Macromolecules* **2004**, 37, 4922-4930.

[33] Hervé, P.; Destarac, M.; Berret, J. F.; Lal, J.; Oberdisse, J.; Grillo, I. *Europhys. Lett*. **2002**, 58, 912-918.

[34] Bronich, T.K.; Nehls, A.; Eisenberg, A.; Kabanov, V.A.; Kabanov, A.V. *Colloid. Surf. B Biointerfaces* **1999**, 16, 243-251.

[35] Uhrich, K. E.; Cannizzaro, S. M.; Langer, R. S.; Shakesheff, K. M. *Chem. Rev*. **1999**, 99, 3181-3198.

[36] Allen et al. *Bioscience Reports* **2002**, 22, 225-250.

[37] Mountrichas, G.; Pispas, S. *J. Polym. Sci. A Polym. Chem.* **2007**, 45, 5790-5799.

[38] Štěpánek M., Hajduová J., Procházka K., Šlouf M., Nebesářová J., Mountrichas, G., Mantzaridis C., Pispas S. *Langmuir* **2012**, 28, 307-313.

[39] Hammouda, B.; Ho, D. L.; Kline, S. *Macromolecules* **2004**, 37, 6932-6937.

[40] Filippov, S. K.; Lezov, A. V.; Sergeeva, O. Yu.; Olifirenko, A. S.; Lesnichin, S. B.; Domnina, N. S.; Komarova, E. A.; Almgren, M.; Karlsson, G.; Štěpánek, P. *Eur. Polym. J.* **2008**, 44, 3361-3369.

[41] Štěpánek, M.; Matějíček, P.; Procházka, K.; Filippov, S. K.; Angelov, B.; Šlouf, M.; Mountrichas, G.; Pispas, S. *Langmuir* **2011**, 27, 5275-5281.

[42] Yun, S. I.; Briber, R. M.; Kee, A. R.; Gauthier, M. *Polymer* **2006**, 47, 2750-2759.

[43] Devanand, K.; Selser, *J. C. Nature* **1990**, 343, 739-741.

[44] Polik, W. F.; Burchard, W. *Macromolecules* **1983**, 16, 978-982.